Journal of Computational Physics **160,** 597–611 (2000)
doi:10.1006/jcph.2000.6476, available online at http://www.idealibrary.com on IDEAL®

A Weak Form of the Conjugate Gradient FFT Method for Two-Dimensional Elastodynamics

George Pelekanos,* Ralph E. Kleinman,†,[1] and Peter M. van den Berg‡

*Department of Mathematics and Statistics, Southern Illinois University, Edwardsville, Illinois 62026;
†Department of Mathematical Sciences, University of Delaware, Newark, Delaware 19716;
and ‡Laboratory of Electromagnetic Research, Faculty of Electrical Engineering,
Delft University of Technology, Delft, The Netherlands
E-mail: *gpeleka@siue.edu

Received August 13, 1999; revised February 22, 2000

The problem of two-dimensional scattering of elastic waves by an elastic inclusion can be formulated in terms of a domain integral equation, in which the grad-div operator acts on a vector potential. The vector potential is the spatial convolution of a Green's function with the product of the density and the displacement over the domain of interest. A weak form of the integral equation for the unknown displacement is obtained by testing it with rooftop functions. This method shows excellent numerical performance.

1. INTRODUCTION

The problem of elastic scattering by an inhomogeneous isotropic object can be formulated in terms of an integral equation for the displacement over the domain of the object. This integral equation can be written in a form where a grad-div operator acts on a vector potential. The vector potential is the spatial convolution of a Green's function with the product of the density and the displacement over the domain of interest.

Numerous methods have been developed in electromagnetics to solve similar domain integral equations. Among those, we choose to implement the k-space methods, since we believe that methods of this type can be used for the solution of three-dimensional problems due to their storage and computational efficiency.

According to [25] the first method for solving the electric field integral equation over the domain of a dielectric object was developed by Richmond [16, 17]. He used the method of moments with pulse expansion functions and point matching. The method of moments, however, is computationally expensive since an inversion of a large matrix is necessary. To

[1] Deceased.

0021-9991/00 $35.00

be more precise, it is known that direct solution of a system of equations in the method of moments needs $\frac{1}{3}N^3$ computations, where N is the number of unknowns. In our method we do not solve a system and our computation time is $n \times N \log(N)$, where n is the number of iterations.

Bojarski [4] introduced the k-space method, in which a fast Fourier transform algorithm for computation of the spatial convolution that occurs in the integral equation reduced the storage and computation time. As a result, the conjugate gradient method combined with the fast Fourier transform (FFT) was developed [19, 21].

However, Borup *et al*. [5] showed that in the conjugate gradient FFT method serious inaccuracies are observed for cylindrical objects in the TE case, and they adequately explained the source of the problem. In 1990 Joachimowicz and Pichot [9] introduced a domain integral equation using generalized functions. Their approach improved the existing numerical results. However, some problems were still observed. For completeness we refer the interested reader to [6, 18, 20]. In order to avoid these difficulties we use a weak form of the conjugate gradient FFT method by testing the integral equation with rooftop functions. Subsequently, a suitable expansion procedure of the vector potential in the integral equation is carried out. The grad-div operator acting on the vector potential of the integral equation is integrated analytically over the object domain. Because of our simple convolution structure the computational time has been significantly reduced. This approach was first introduced by Van den Berg and Zwamborn [24, 25] in electromagnetics and gave very accurate numerical results.

We choose 2-D formulations to test our algorithm because they are less computationally involved than 3-D ones.

The numerical results presented are compared with analytical solutions, and it is demonstrated that the present method shows excellent results. The first attempt at comparison between the approximate and analytical solution was made by Banaugh in his Ph.D. thesis [2]; see also [3]. Banaugh used boundary integral equations expressed in terms of a set of displacement potentials. The equations are solved by means of finite difference approximations to the contour integrals. The resulting scattered field was found to be in excellent agreement with that obtained from the series solution. In this way, Banaugh has obtained numerical values for the surface potentials in the case of two-dimensional rigid and elastic cylinders of arbitrary cross section. However, the numerical results presented involved only small wave numbers ($k_p = 1, k_s = 2$). Calculations for larger values of k have not been executed since the necessary increase in matrix size results in excessive computational effort [3].

2. NOTATION AND STATEMENT OF THE PROBLEM

Let C be a closed, Lyapunov curve in $\mathbb{R}^2$ in the sense of Kupradze [11], on which a Hölder continuous normal exists everywhere. Let D_i and D_e denote the regions interior and exterior to C. Erect a Cartesian coordinate system with origin in D_i and denote points in $\mathbb{R}^2$ as $\mathbf{x} = (x_1, x_2)$ and $\mathbf{x}' = (x_1', x_2')$. Assume that D_i is filled with an inhomogeneous elastic material characterized by the constant Lame coefficients λ and μ.

Let the source point $\mathbf{x}_*$ belong to domain D_e. Let $\mathbf{u}^{\text{inc}}$ be the displacement field to which the given source gives rise throughout the domain D_e, which is filled with a homogeneous elastic material, also characterized by the constants λ and μ.

The forward scattering problem is modelled by the following transmission problem (TP). For a given incident field $\mathbf{u}^{\text{inc}}$ and zero body forces, determine $\mathbf{u}(\mathbf{x})$ such that

$$\Delta^* \mathbf{u}^i(\mathbf{x}) + \rho(\mathbf{x})\omega^2 \mathbf{u}^i(\mathbf{x}) = 0, \qquad \mathbf{x} \in D_i \tag{1}$$

$$\Delta^* \mathbf{u}^e(\mathbf{x}) + \rho_e \omega^2 \mathbf{u}^e(\mathbf{x}) = 0, \qquad \mathbf{x} \in D_e \tag{2}$$

$$\mathbf{u}^i(\mathbf{x}) = \mathbf{u}^e(\mathbf{x}), \qquad \mathbf{x} \in S \tag{3}$$

$$\mathbf{T}\mathbf{u}^i(\mathbf{x}) = \mathbf{T}\mathbf{u}^e(\mathbf{x}), \qquad \mathbf{x} \in S \tag{4}$$

$$\mathbf{u}^{\text{sct}} = \mathbf{u}^e - \mathbf{u}^{\text{inc}} \qquad \text{is regular in } D_e \text{ in the sense of Kupradze.} \tag{5}$$

Here the real density $\rho(\mathbf{x})$ is piecewise Hölder continuous in D_i. Furthermore, the operator Δ^* is defined as

$$\Delta^* \equiv (\lambda + 2\mu)\nabla\nabla - \mu\nabla \times \nabla \times, \tag{6}$$

and the stress operator $\mathbf{T}$ is defined as (Ahner and Hsiao [1])

$$\begin{aligned}\mathbf{T}\mathbf{u}(\mathbf{x}) = &\left\{\left[(\lambda + 2\mu)\frac{\partial u_1}{\partial x_1} + \lambda\frac{\partial u_2}{\partial x_2}\right]\cos(\hat{\mathbf{n}}, x_1) + \mu\left[\frac{\partial u_1}{\partial x_2} + \frac{\partial u_2}{\partial x_1}\right]\cos(\hat{\mathbf{n}}, x_2)\right\}\hat{\mathbf{e}}_1 \\ &+ \left\{\mu\left[\frac{\partial u_1}{\partial x_2} + \frac{\partial u_2}{\partial x_1}\right]\cos(\hat{\mathbf{n}}, x_1) + \left[\lambda\frac{\partial u_1}{\partial x_1} + (\lambda + 2\mu)\frac{\partial u_2}{\partial x_2}\right]\cos(\hat{\mathbf{n}}, x_2)\right\}\hat{\mathbf{e}}_2.\end{aligned} \tag{7}$$

It can be shown [10, 13] that the above problem is governed by the integral equation

$$\mathbf{u}(\mathbf{x}) = \mathbf{u}^{\text{inc}}(\mathbf{x}) + \omega^2 \int_{D_i} (\rho(\mathbf{x}') - \rho_e)\mathbf{u}(\mathbf{x}') \cdot \mathbf{\Gamma}(\mathbf{x}, \mathbf{x}')\, dv_{\mathbf{x}'}, \qquad \mathbf{x} \in \mathbb{R}^2, \tag{8}$$

where $\mathbf{\Gamma}(\mathbf{x}, \mathbf{x}')$ is the Green's displacement tensor and is given by Morse and Feshbach [12] as

$$\mathbf{\Gamma}(\mathbf{x}, \mathbf{x}') = \frac{i}{4}\left\{\frac{1}{\mu}\mathbf{I}H_0^{(1)}(k_s|\mathbf{x} - \mathbf{x}'|) - \frac{1}{\omega^2\rho_e}\nabla\nabla\left[H_0^{(1)}(k_p|\mathbf{x} - \mathbf{x}'|) - H_0^{(1)}(k_s|\mathbf{x} - \mathbf{x}'|)\right]\right\}, \tag{9}$$

where k_p, k_s are the wave numbers for the P and the S wave, respectively.

The uniqueness of the solution $\mathbf{u}(\mathbf{x})$ to this problem can be found in Kupradze [11] and Hähner [8].

Inserting Eq. (9) into (8) yields

$$\begin{aligned}\mathbf{u}^{\text{inc}}(\mathbf{x}) = \mathbf{u}(\mathbf{x}) &- k_s^2 \int_{D_i} \frac{i}{4}H_0^{(1)}(k_s|\mathbf{x} - \mathbf{x}'|)\mathcal{M}(\mathbf{x}')\mathbf{u}(\mathbf{x}')\, dv_{\mathbf{x}'} \\ &- \nabla\nabla \cdot \int_{D_i} \frac{i}{4}\left[H_0^{(1)}(k_s|\mathbf{x} - \mathbf{x}'|) - H_0^{(1)}(k_p|\mathbf{x} - \mathbf{x}'|)\right]\mathcal{M}(\mathbf{x}')\mathbf{u}(\mathbf{x}')\, dv_{\mathbf{x}'},\end{aligned} \tag{10}$$

where

$$\mathcal{M}(\mathbf{x}') = \frac{\rho(\mathbf{x}') - \rho_e}{\rho_e}. \tag{11}$$

The integral equation above now takes the form

$$u_1^{\text{inc}} = u_1 - B_1, \qquad (x_1, x_2) \in D_i, \tag{12}$$

$$u_2^{\text{inc}} = u_2 - B_2, \qquad (x_1, x_2) \in D_i, \tag{13}$$

where the components B_1 and B_2 of the vector $\mathbf{B}$ are given by

$$B_1 = k_s^2 C_1 + \partial_1[\partial_1 A_1 + \partial_2 A_2], \tag{14}$$

$$B_2 = k_s^2 C_2 + \partial_2[\partial_1 A_1 + \partial_2 A_2], \tag{15}$$

in which ∂_α denotes the partial derivative with respect to x_α, $\alpha = 1, 2$ and the vector potentials,

$$\mathbf{A} = \{A_1(x_1, x_2), A_2(x_1, x_2)\}, \qquad \mathbf{C} = \{C_1(x_1, x_2), C_2(x_1, x_2)\}, \tag{16}$$

are given by

$$\mathbf{A}(x_1, x_2) = \int_{(x_1', x_2') \in D_i} \Gamma_{s,p}(x_1 - x_1', x_2 - x_2') \mathcal{M}(x_1', x_2') \mathbf{u}(x_1', x_2')\, dx_1'\, dx_2', \tag{17}$$

where

$$\Gamma_{s,p}(x_1 - x_1', x_2 - x_2') = \frac{i}{4}\left[H_0^{(1)}(k_s|\mathbf{x} - \mathbf{x}'|) - H_0^{(1)}(k_p|\mathbf{x} - \mathbf{x}'|)\right] \tag{18}$$

and

$$\mathbf{C}(x_1, x_2) = \int_{(x_1', x_2') \in D_i} \Gamma_s(x_1 - x_1', x_2 - x_2') \mathcal{M}(x_1', x_2') \mathbf{u}(x_1', x_2')\, dx_1'\, dx_2', \tag{19}$$

where

$$\Gamma_s(x_1 - x_1', x_2 - x_2') = \frac{i}{4} H_0^{(1)}(k_s|\mathbf{x} - \mathbf{x}'|). \tag{20}$$

3. THE DISCRETIZATION PROCEDURE

We now proceed with the discretization by assuming that the domain D_i is a rectangular domain with boundaries along the x_1 and x_2 directions. We use a rectangular mesh with a grid width of Δx_1 in the x_1 direction and Δx_2 in the x_2 direction.

The rectangular subdomains created are given by

$$D_{m,n} = \{(x_1, x_2) \in \mathbb{R}^2 \mid x_{1;m-1} < x_1 < x_{1;m}, x_{2;n-1} < x_2 < x_{2;n}\}, \tag{21}$$

where

$$x_{1;m} = x_{1;M-1} + m\Delta x_1, \qquad m = 1, \ldots, M, \tag{22}$$

$$x_{2;n} = x_{2;N-1} + n\Delta x_2, \qquad n = 1, \ldots, N, \tag{23}$$

in which $x_{1;0}$ is the lower x_1 bound of the contrasting domain D_i, while $x_{2;0}$ is its lower x_2 bound. We assume that the boundary of the domain is located in the embedding where $\mathcal{M} = 0$. It is understood that this is possible since the scattering domain can be extended with a zero contrast function $\mathcal{M}$. In each rectangular subdomain $D_{m,n}$ with center $(x_{1;m-1/2}, x_{2;n-1/2})$ we assume the real contrast $\mathcal{M}$ to be constant with value $\mathcal{M}_{m,n}$.

We define two sequences of basis functions over the domain D_i: a sequence $\psi^{(1)}_{m,n}(x_1, x_2)$ that is continuous in the x_1 direction and may jump at discontinuities of the material distribution in the x_2 direction, and a sequence $\psi^{(2)}_{m,n}(x_1, x_2)$ that is continuous in the x_2 direction and may jump at discontinuities of the density distribution in the x_1 direction; see [22]. The most simple basis functions that meet these requirements are the rooftop functions and are defined as [13, 25]

$$\psi^{(1)}_{m,n}(x_1, x_2) = \Lambda(x_1 - x_{1;m} \mid \Delta x_1, \Delta x_1)\, \Pi\big(x_2 - x_{2;n-1/2} \,\big|\, \Delta x_2\big), \tag{24}$$

for $m = 1, \ldots, M-1$ and $n = 2, \ldots, N-1$, and

$$\psi^{(2)}_{m,n}(x_1, x_2) = \Pi\big(x_1 - x_{1;m-1/2} \,\big|\, \Delta x_1\big)\, \Lambda(x_2 - x_{2;n} \mid \Delta x_2, \Delta x_2), \tag{25}$$

for $m = 2, \ldots, M-1$ and $n = 1, \ldots, N-1$. In the above $\Lambda(x_1 - x_{1;m} \mid \Delta x_1, \Delta x_1)$ is the triangle function with support $2\Delta x_1$ and $\Pi(x_1 - x_{1;m-1/2} \mid \Delta x_1)$ is the pulse function with support Δx_1. We further define

$$u_{1;m,n} = u_1\big(x_{1;m}, x_{2;n-1/2}\big), \tag{26}$$

$$u^{\text{inc}}_{1;m,n} = u^{\text{inc}}_1\big(x_{1;m}, x_{2;n-1/2}\big), \tag{27}$$

$$B_{1;m,n} = B_1\big(x_{1;m}, x_{2;n-1/2}\big), \tag{28}$$

$$\mathcal{M}_{m+1/2,n} = \frac{1}{2}\mathcal{M}_{m,n} + \frac{1}{2}\mathcal{M}_{m+1,n}, \tag{29}$$

for $m = 1, \ldots, M-1$ and $n = 2, \ldots, N-1$, and

$$u_{2;m,n} = u_2\big(x_{1;m-1/2}, x_{2;n}\big), \tag{30}$$

$$u^{\text{inc}}_{2;m,n} = u^{\text{inc}}_2\big(x_{1;m-1/2}, x_{2;n}\big), \tag{31}$$

$$u_{2;m,n} = u_2\big(x_{1;m-1/2}, x_{2;n}\big), \tag{32}$$

$$\mathcal{M}_{m,n+1/2} = \frac{1}{2}\mathcal{M}_{m,n} + \frac{1}{2}\mathcal{M}_{m,n+1}, \tag{33}$$

for $m = 2, \ldots, M-1$ and $n = 1, \ldots, N-1$.

Then Eqs. (12)–(13) are discretized as

$$U_{1;m,n} - B_{1;m,n} = u^{\text{inc}}_{1;m,n}, \tag{34}$$

$$U_{2;m,n} - B_{2;m,n} = u^{\text{inc}}_{2;m,n}. \tag{35}$$

We now replace Eqs. (14)–(15) by their weak versions

$$B_{1;m,n} = \frac{\int_{\mathbf{x}\in(D_{m,n}\cup D_{m+1,n})} \psi^{(1)}_{m,n}(x_1,x_2)\{k_s^2 C_1 + \partial_1[\partial_1 A_1 + \partial_2 A_2]\}\,\mathrm{dv}}{\int_{\mathbf{x}\in(D_{m,n}\cup D_{m+1,n})} \psi^{(1)}_{m,n}(x_1,x_2)\,\mathrm{dv}}, \tag{36}$$

$$B_{2;m,n} = \frac{\int_{\mathbf{x}\in(D_{m,n}\cup D_{m,n+1})} \psi^{(2)}_{m,n}(x_1,x_2)\{k_s^2 C_2 + \partial_2[\partial_1 A_1 + \partial_2 A_2]\}\,\mathrm{dv}}{\int_{\mathbf{x}\in(D_{m,n}\cup D_{m,n+1})} \psi^{(2)}_{m,n}(x_1,x_2)\,\mathrm{dv}}, \tag{37}$$

while the vector potentials **A** and **C** are explanded as

$$A_1(x_1,x_2) = \sum_{p,q} A_{1;p,q}\psi^{(1)}_{p,q}(x_1,x_2), \tag{38}$$

$$A_2(x_1,x_2) = \sum_{p,q} A_{2;p,q}\psi^{(2)}_{p,q}(x_1,x_2). \tag{39}$$

$$C_1(x_1,x_2) = \sum_{p,q} C_{1;p,q}\psi^{(1)}_{p,q}(x_1,x_2), \tag{40}$$

$$C_2(x_1,x_2) = \sum_{p,q} C_{2;p,q}\psi^{(2)}_{p,q}(x_1,x_2). \tag{41}$$

We then obtain

$$B_{1;m,n} = \sum_{p=0}^{M}\sum_{q=1}^{N} g_{m,n,p,q}C_{1;p,q} + \sum_{p=0}^{M}\sum_{q=1}^{N} a_{m,n,p,q}A_{1;p,q} + \sum_{p=1}^{M}\sum_{q=0}^{N} b_{m,n,p,q}A_{2;p,q}, \tag{42}$$

$$B_{2;m,n} = \sum_{p=0}^{M}\sum_{q=1}^{N} h_{m,n,p,q}C_{2;p,q} + \sum_{p=1}^{M}\sum_{q=0}^{N} c_{m,n,p,q}A_{2;p,q} + \sum_{p=0}^{M}\sum_{q=1}^{N} d_{m,n,p,q}A_{1;p,q}, \tag{43}$$

where

$$g_{m,n,p,q} = \frac{1}{6}k_s^2(\delta_{p,m+1} + 4\delta_{p,m} + \delta_{p,m-1})\delta_{q,n}, \tag{44}$$

$$a_{m,n,p,q} = (\Delta x_1)^{-2}(\delta_{p,m+1} - 2\delta_{p,m} + \delta_{p,m-1})\delta_{q,n}, \tag{45}$$

$$b_{m,n,p,q} = (\Delta x_1\Delta x_2)^{-1}(\delta_{p,m-1} - \delta_{p,m})(\delta_{q,n} - \delta_{q,n+1}), \tag{46}$$

$$h_{m,n,p,q} = \frac{1}{6}k_s^2(\delta_{q,n+1} + 4\delta_{q,n} + \delta_{q,n-1})\delta_{p,m}, \tag{47}$$

$$c_{m,n,p,q} = (\Delta x_2)^{-2}(\delta_{q,n+1} - 2\delta_{q,n} + \delta_{q,n-1})\delta_{p,m}, \tag{48}$$

$$d_{m,n,p,q} = (\Delta x_1\Delta x_2)^{-1}(\delta_{p,m+1} - \delta_{p,m})(\delta_{q,n} - \delta_{q,n-1}), \tag{49}$$

in which $\delta_{m,n}$ is the Kronecker delta [13].

Subsequently Eqs. (42) and (43) become

$$B_{1;m,n} = \frac{1}{6}k_s^2(C_{1;m-1,n} + 4C_{1;m,n} + C_{1;m+1,n}) + (\Delta x_1)^{-2}(A_{1;m-1,n} - 2A_{1;m,n} + A_{1;m+1,n}) + (\Delta x_1\Delta x_2)^{-1}(A_{2;m,n-1} - A_{2;m,n} + A_{2;m+1,n} - A_{2,m+1,n-1}), \tag{50}$$

$$B_{2;m,n} = \frac{1}{6}k_s^2(C_{2;m,n-1} + 4C_{2;m,n} + C_{2;m,n+1}) + (\Delta x_2)^{-2}(A_{2;m,n-1} - 2A_{2;m,n} + A_{2,m,n+1}) + (\Delta x_1 \Delta x_2)^{-1}(A_{1;m-1,n} - A_{1;m,n} + A_{1;m,n+1} - A_{1,m-1,n+1}). \quad (51)$$

We now need to replace the continuous representations of the vector potentials **A** and **C** by discrete ones. In order to cope with the singularity of Γ_s we use a global representation consistent with our weak formulation. We integrate C_1 over a circular domain with center at the point $(x_{1;m}, x_{2;n-1/2})$, and C_2 over a circular domain with center at the point $(x_{1;m-1/2}, x_{2;n})$. For consistency we repeat the above procedure for the vector potentials A_1 and A_2, respectively. The radius of the circular patches is taken to be $\frac{1}{2}\Delta x = \frac{1}{2}\min(\Delta x_1, \Delta x_2)$. The results are divided by the surface area $\pi(\frac{1}{2}\Delta x)^2$ [16].

After approximating the resulting intergrals by appropriate trapezoidal rules we obtain

$$C_{1;m,n} = \Delta x_1 \Delta x_2 \sum_{m'=1}^{M-1}\sum_{n'=2}^{N-1} \Gamma_s^*\left(x_{1;m} - x_{1;m'}, x_{2;n-1/2} - x_{2;n'-1/2}\right)\mathcal{M}_{m'+1/2,n'}u_{1;m',n'}, \quad (52)$$

for $m = 0, \ldots, M$ and $n = 1, \ldots, N$,

$$C_{2;m,n} = \Delta x_1 \Delta x_2 \sum_{m'=2}^{M-1}\sum_{n'=1}^{N-1} \Gamma_s^*\left(x_{1;m-1/2} - x_{1;m'-1/2}, x_{2;n} - x_{2;n'}\right)\mathcal{M}_{m',n'+1/2}u_{2;m',n'}, \quad (53)$$

for $m = 1, \ldots, M$ and $n = 0, \ldots, N$,

$$A_{1;m,n} = \Delta x_1 \Delta x_2 \sum_{m'=1}^{M-1}\sum_{n'=2}^{N-1} \Gamma_{s,p}^*\left(x_{1;m} - x_{1;m'}, x_{2;n-1/2} - x_{2;n'-1/2}\right)\mathcal{M}_{m'+1/2,n'}u_{1;m',n'}, \quad (54)$$

for $m = 0, \ldots, M$ and $n = 1, \ldots, N$, and

$$A_{2;m,n} = \Delta x_1 \Delta x_2 \sum_{m'=2}^{M-1}\sum_{n'=1}^{N-1} \Gamma_{s,p}^*\left(x_{1;m-1/2} - x_{1;m'-1/2}, x_{2;n} - x_{2;n'}\right)\mathcal{M}_{m'n'+1/2}u_{2;m',n'}, \quad (55)$$

for $m = 1, \ldots, M$ and $n = 0, \ldots, N$, where $\Gamma_{s,p}^*$ and Γ_s^* are the integrals of the corresponding Green's functions $\Gamma_{s,p}$ and Γ_s over the circular patches discussed above and are divided by the surface area $\pi(\frac{1}{2}\Delta x)^2$. The discrete convolutions $C_{1;m,n}$, $C_{2;m,n}$, $A_{1;m,n}$ and $A_{2;m,n}$ can be computed effeciently using FFT routines [15].

4. SOLUTION OF THE PROBLEM

We now substitute Eqs. (52)–(55) into Eqs. (42)–(43) and use the results in Eqs. (34)–(35).

This yields a linear system of equations for $u_{1;m,n}$ and $u_{2;m,n}$ with known $\mathcal{M}$; i.e.,

$$(\mathbf{Lu})_{1;p,q} = u_{1;p,q}^{\text{inc}}, \qquad p = 1, \ldots, M-1, \qquad q = 2, \ldots, N-1, \quad (56)$$

$$(\mathbf{Lu})_{2;p,q} = u_{2;p,q}^{\text{inc}}, \qquad p = 2, \ldots, M-1, \qquad q = 1, \ldots, N-1, \quad (57)$$

where

$$(\mathbf{Lu})_{1;p,q} = u_{1;p,q} - \sum_{m=0}^{M}\sum_{n=0}^{N} g_{p,q,m,n}C_{1;m,n} - \sum_{m=0}^{M}\sum_{n=1}^{N} a_{p,q,m,n}A_{1;m,n} - \sum_{m=1}^{M}\sum_{n=0}^{N} b_{p,q,m,n}A_{2;m,n}, \tag{58}$$

for $p = 1, \ldots, M-1$ and $q = 2, \ldots, N-1$, and

$$(\mathbf{Lu})_{2;p,q} = u_{2;p,q} - \sum_{m=1}^{M}\sum_{n=0}^{N} h_{p,q,m,n}C_{2;m,n} - \sum_{m=1}^{M}\sum_{n=0}^{N} c_{p,q,m,n}A_{2;m,n} - \sum_{m=0}^{M}\sum_{n=1}^{N} d_{p,q,m,n}A_{1;m,n}, \tag{59}$$

for $p = 2, \ldots, M-1$ and $q = 1, \ldots, N-1$, and where $A_{1;m,n}$, $A_{2;m,n}$, $C_{1;m,n}$, and $C_{2;m,n}$ directly follow from Eqs. (52)–(55).

The operator equation given by (56)–(57) will be solved with the aid of the conjugate gradient method; see [21] and [13, p. 35].

For convenience, the P (dilation) and SV (rotation) components of the two-dimensional scattered field are introduced [7].

The scattered P component is given by

$$u_p^{\mathrm{sct}}(\mathbf{x}) = \partial_1 u_1^{\mathrm{sct}}(\mathbf{x}) + \partial_2 u_2^{\mathrm{sct}}(\mathbf{x}) \qquad \mathbf{x} \in S. \tag{60}$$

Consequently the scattered SV component is given by

$$u_s^{\mathrm{sct}}(\mathbf{x}) = \partial_1 u_2^{\mathrm{sct}}(\mathbf{x}) - \partial_2 u_1^{\mathrm{sct}}(\mathbf{x}), \qquad \mathbf{x} \in S. \tag{61}$$

Detailed forms for the above component equations can be found in [13].

5. NUMERICAL RESULTS

In our first numerical example the scatterer was taken to be a circular cylinder of radius $a = 0.35$ m and density $\rho = 1.3$, while the outer medium's density was 1; see also Fig. 1. Hence, the contrast is 0.3. The scatterer is located in the test square D_i. This test square

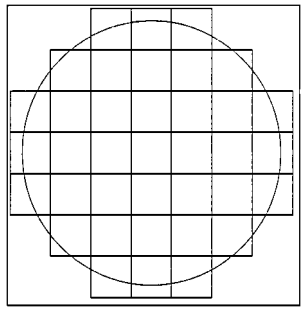

FIG. 1. Discretization of the circular cylinder.

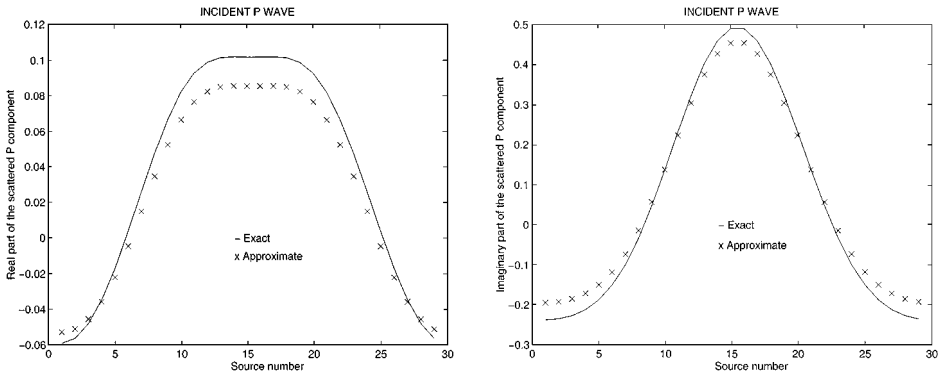

FIG. 2. The real and the imaginary parts of the P component of the scattered field at the first station for $k_p = 3$, $k_s = 6$, Err $= 10^{-2}$, and 21×21 subsquares.

was divided into 21×21 subsquares of $0.1 \times 0.1\,\mathrm{m}^2$. The wave numbers of the P-waves and the SV-waves are $k_p = 3$, $k_s = 6$, respectively. This means that the sidelength of the test square was equal to about one wavelength for the P-waves and two wavelengths for the SV-waves in the exterior medium. We excite our object by either P-waves or SV-waves. The object will scatter both P-waves and SV-waves. The measurement surface S was chosen to be a circle with a radius of 3 m. Twenty-nine stations ($J = 29$) were located uniformly on this circle, with each station serving successively as a line source and all stations acting as receivers. The DFTs are efficiently computed using FFT algorithms [15].

In Figs. 2 and 3 we present the real and the imaginary parts of the P and SV components of the scattered field, respectively. The tolerance in the residual error norm is taken to be 1%. Comparison with the analytical solution—see [23] and [13]—is made, and it follows that a tolerance of 1% in the residual norm is insufficient.

We now repeat the above numerical experiment but this time for SV wave incidence. In Figs. 4 and 5 we have recorded the real and imaginary parts of the P and SV components of the scattered field, respectively. Again comparison with the exact solution is made. It follows that the above tolerance is also insufficient.

We now repeat the above numerical experiment but this time with tolerance in the residual norm of 0.1%. Comparison with the analytical solution, which is made in Figs. 6–9, shows

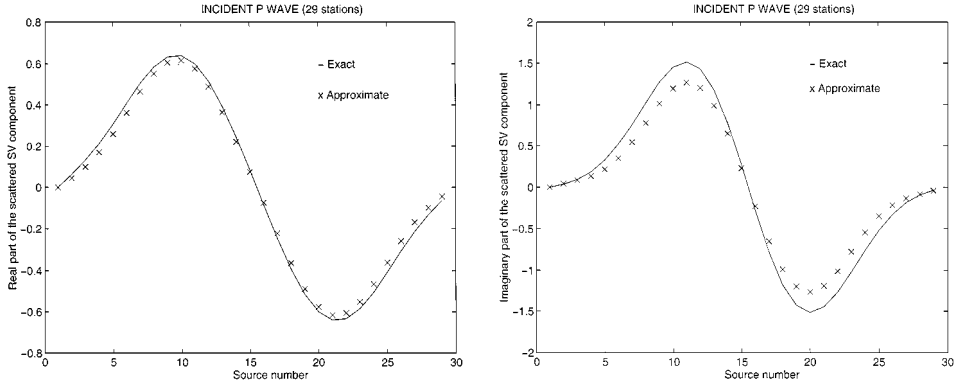

FIG. 3. The real and the imaginary parts of the SV component of the scattered field at the first station for $k_p = 3$, $k_s = 6$, Err $= 10^{-2}$, and 21×21 subsquares.

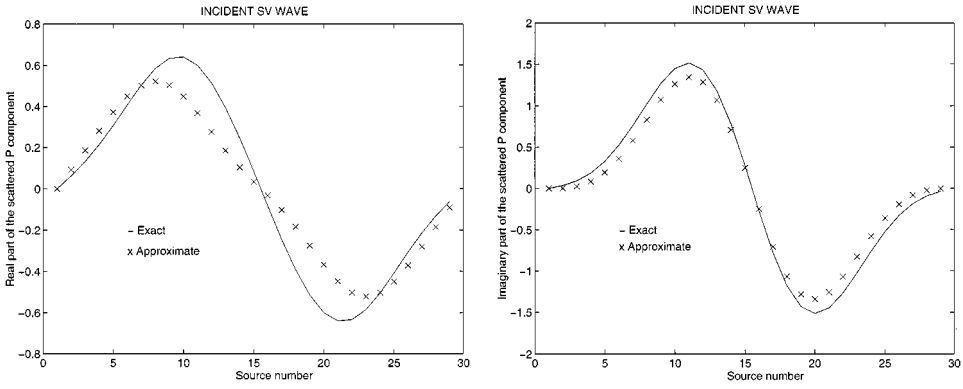

FIG. 4. The real and the imaginary parts of the P component of the scattered field at the first station for $k_p = 3$, $k_s = 6$, Err $= 10^{-2}$, and 21×21 subsquares.

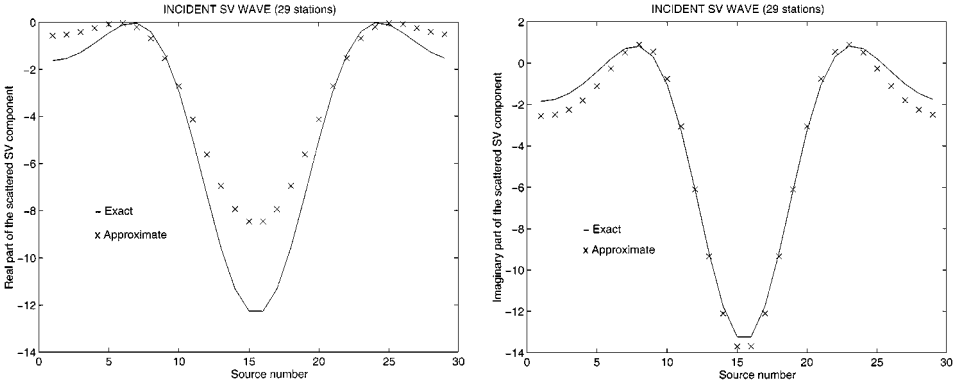

FIG. 5. The real and the imaginary parts of the SV component of the scattered field at the first station for $k_p = 3$, $k_s = 6$, Err $= 10^{-2}$, and 21×21 subsquares.

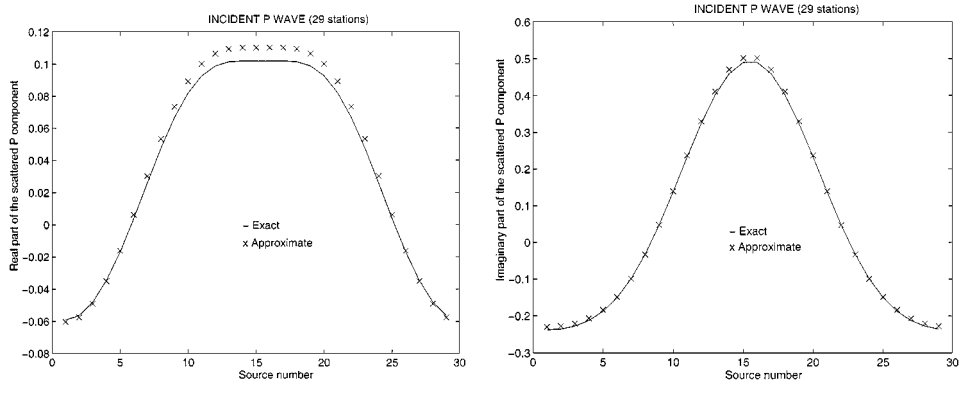

FIG. 6. The real and the imaginary parts of the P component of the scattered field at the first station for $k_p = 3$, $k_s = 6$, Err $= 10^{-3}$, and 21×21 subsquares.

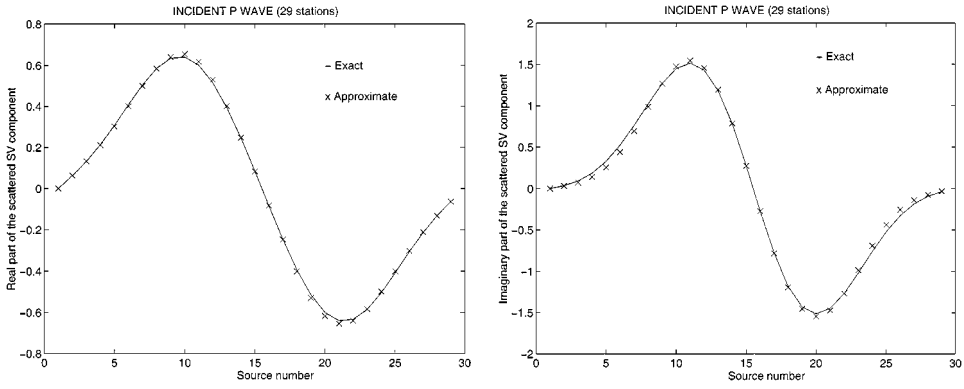

FIG. 7. The real and the imaginary parts of the SV component of the scattered field at the first station for $k_p = 3$, $k_s = 6$, Err $= 10^{-3}$, and 21×21 subsquares.

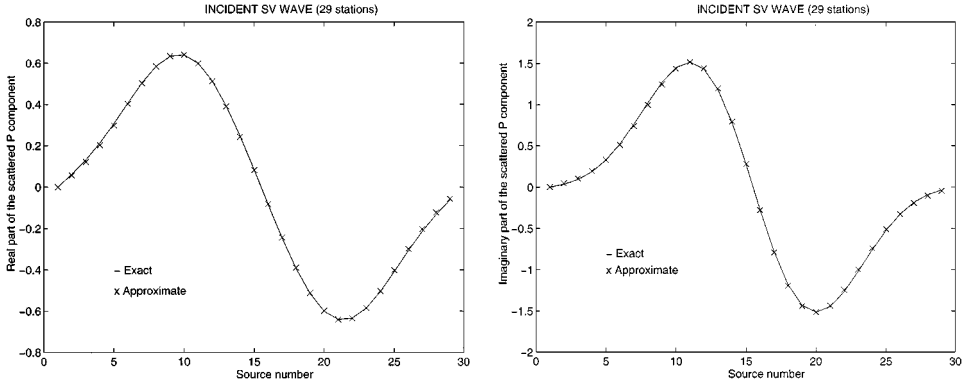

FIG. 8. The real and the imaginary parts of the P component of the scattered field at the first station for $k_p = 3$, $k_s = 6$, Err $= 10^{-3}$, and 21×21 subsquares.

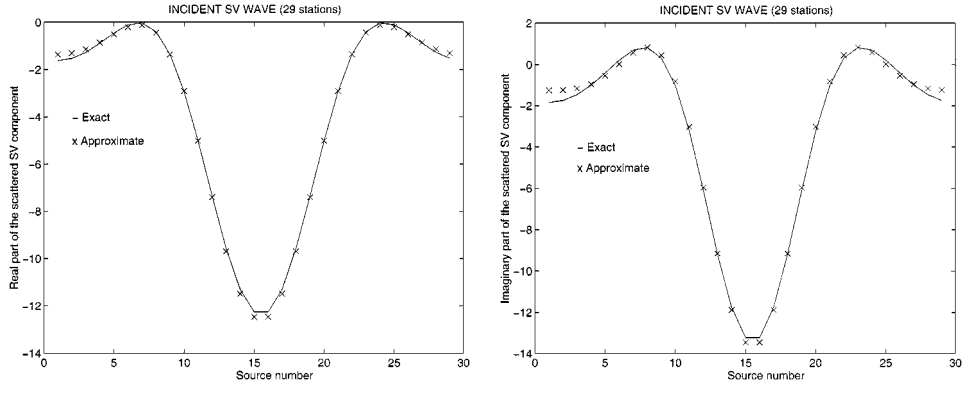

FIG. 9. The real and the imaginary parts of the SV component of the scattered field at the first station for $k_p = 3$, $k_s = 6$, Err $= 10^{-3}$, and 21×21 subsquares.

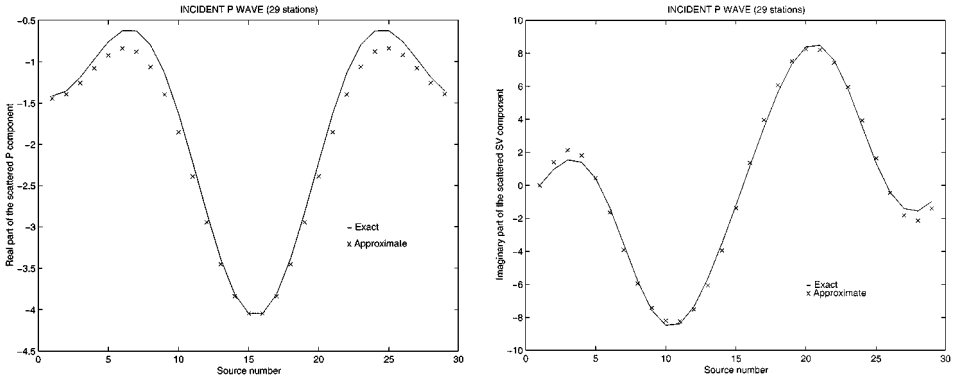

FIG. 10. The real and imaginary parts of the P and SV component of the scattered field, respectively, at the first station for $k_p = 3$, $k_s = 6$, contrast 6.3, Err $= 10^{-3}$, and 41×41 subsquares.

excellent numerical results for both kinds of wave incidence. The above tolerance is achieved with only six iterations. We can now state that a tolerance of 0.1% is sufficient for the same mesh since repeating the present experiment with tolerance of 0.01% yields identical numerical results.

We now continue our numerical experiments by considering a problem with same geometry as the previous one, but with higher contrast. Assume now that the density of the scatterer is now increased to $\rho = 7.3$ and hence the contrast is 6.3. We excite our object by a P-wave. It turns out that division of our domain in 21×21 subsquars is not sufficient, so we increase their number to 41×41. For brevity in Fig. 10 we present only the real and imaginary parts of the P and SV components of the scattered field, respectively. As it was expected the number of iterations has now been significantly increased. It is worthwile to point out that when the contrast was 0.3, only seven iterations were enough to achieve the desired accuracy (10^{-3}), but now this number has been increased to 92; see Fig. 11. It is hence observed, that increase in the value of the contrast results to a significant increase in the iteration number. In Fig. 12 we show in a log–log scale the graph of $\|u_{\text{approx}} - u_{\text{exact}}\|_\infty$ (where u_{approx} and u_{exact} are the P-components of the scattered field, for the approximate and exact solution respectively) with respect to the mesh size, and

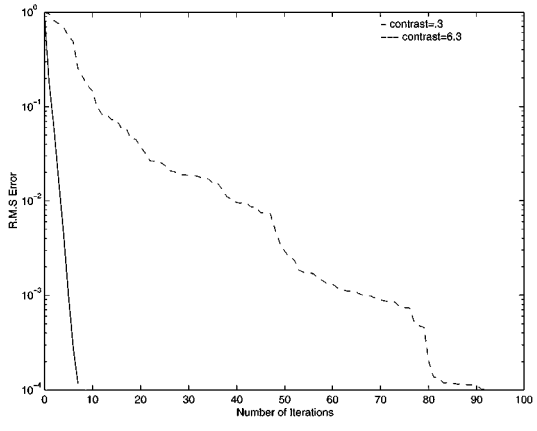

FIG. 11. Comparison between the number of iterations for two different values of the contrast.

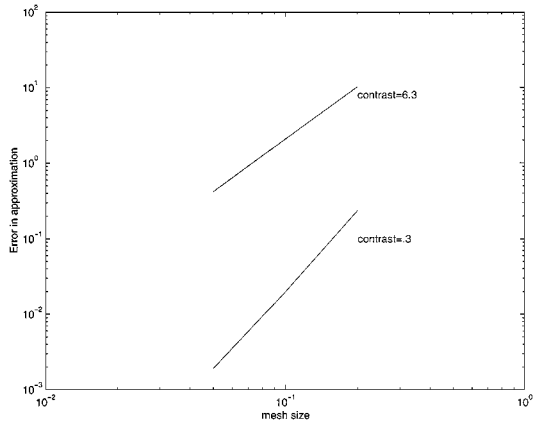

FIG. 12. Plot of $\|u_{\text{approx}} - u_{\text{exact}}\|_\infty$ with respect to the mesh size. Top line has slope 2.3; bottom line has slope 3.6.

it follows that the order of numerical convergence decreases for increasing values of the contrast.

We now continue our numerical experiments by considering a problem with same geometry as the previous one, but with larger wave numbers. Namely, let the wavenumbers of the P-waves and SV-waves now be $k_p = 6$, $k_s = 12$ and the density of the scatterer to be again $\rho = 1.3$. We first excite our object by a P-wave. We divide our test domain first in 21×21 subsquares of $0.1 \times 0.1\ \text{m}^2$ and then to 41×41 subsquares of $0.0466 \times 0.0466\ \text{m}^2$. For brevity in Fig. 13 we present only the real parts of the P and SV components of the scattered field. It is observed that as the number of discretization points becomes larger the approximation is improved. The same thing was also observed, for the real parts of the P and SV components of the scattered field. The number of iterations is also increased from 7 ($k_p = 3$, $k_s = 6$) to 16.

Hence from the above experiments we can conlude that the order of convergence of our method decreases, for increasing values of the contrast and size of the object. Same behavior as in the P-wave incidence case is observed, if we choose to excite the object by an incident SV wave.

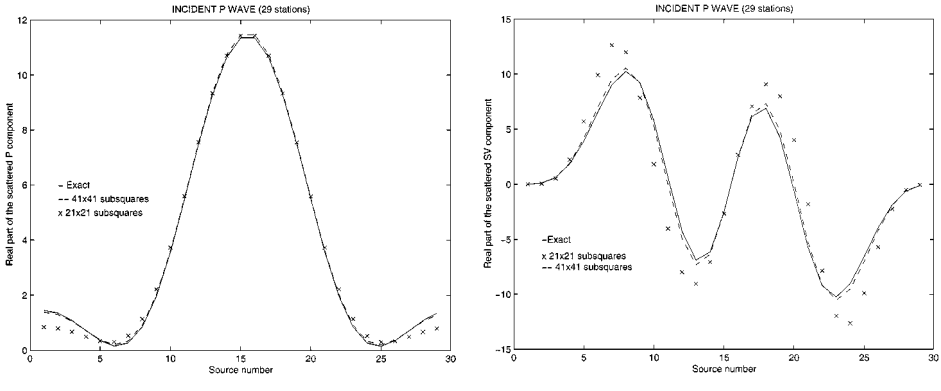

FIG. 13. The real parts of the P and SV component of the scattered field at the first station for $k_p = 6$, $k_s = 12$, and $\text{Err} = 10^{-3}$.

6. CONCLUSIONS

We have presented a weak formulation of the conjugate gradient FFT method for elastic scatterers. It is observed that the present weak form of the conjugate gradient FFT method for the two-dimensional problem yields excellent agreement with the analytical results for the test problems. Modeling the curved boundaries using a rectangular mesh seems to be feasible and discretization errors tend to vanish for increasingly finer discretizations. The simple convolution structure of the vector potential avoided matrix–vector multiplications in the spectral domain. We only have matrix–vector multiplications in the spatial domain, but these are over the domain of the elastic object only. That means that the computation time of our method is even less than the computation time of the conjugate gradient FFT methods discussed in the Introduction.

It is worthwile to mention that triangular discretization with linear expansion functions would give a more accurate result with the same mesh sizes, but the simplicity of the convolution structure of the operator will be lost, and FFT can no longer be used. With a finer discretization of the rectangular domains (with substantially less computation time than using triangular discretization) the same accuracy is achieved.

The present method can provide data which can be used for the solution of the corresponding inverse problem [14]. Future work should also be directed toward extending the method to three-dimensional problems, but this has yet to be done.

ACKNOWLEDGMENT

This work was partially supported under AFOSR Grant F49620-96-1-0039

REFERENCES

1. J. F. Ahner and G. C. Hsiao, On the two-dimensional exterior boundary-value problems of elasticity, *Siam J. Appl. Math.* **31**, 677 (1976).
2. R. P. Banaugh, *Scattering of Elastic Waves by Surfaces of Arbitrary Shape.*, Ph.D. thesis, University of California, Berkeley, 1962.
3. R. P. Banaugh and W. Goldsmith, Diffraction of steady elastic waves by surfaces of arbitrary shape, *J. Appl. Mech*. **30**, 589 (1963).
4. N. N. Bojarski, K-space formulation of the scattering problem in the time domain. *J. Acoust. Soc. Amer.* **72**, 570 (1982).
5. D. T. Borup, D. M. Sullivan, and O. P. Gandhi, Comparison of the FFT conjugate gradient method and the finite-difference time-domain method for the 2-d absorption problem, *IEEE Trans. Microwave Theory Tech.* **MTT-35**, 383 (1987).
6. D. R. Wilton, D. H. Schaubert, and A. W. Glisson, A tetrahedral modeling method for electromagnetic scattering by arbitrarily shaped inhomogeneous dielectric bodies, *IEEE Trans. Antennas Propagat.* **77** (1984).
7. A. C. Eringen and E. S. Suhubi, *Elastodynamics* (Academic Press, New York/San Francisco/London, 1983), Vol. II.
8. P. Hähner, A uniqueness theorem in inverse scattering of elastic waves, *IMA J. Appl. Math.* **51**, 201 (1993).
9. N. Joachimowicz and C. Pichot, Comparison of three formulations for the 2-d TE scattering problem, *IEEE Trans. Microwave Theory Tech*. **38**, 178 (1990).
10. V. D. Kupradze, *Progress in Solid Mechanics* (North-Holland, New York, 1963), Vol. III.
11. V. D. Kupradze, *Potential Methods in the Theory of Elasticity* (Israel Program for Scientific Translations, Jerusalem, 1965).

12. P. M. Morse and H. Feshbach, *Methods of Mathematical Physics* (McGraw–Hill, New York, 1953), Part II.
13. G. Pelekanos, *Direct and Inverse Scattering by an Elastic Inclusion*, Ph.D thesis, University of Delaware, Newark, 1997.
14. G. Pelekanos, R. E. Kleinman, and P. M. van den Berg, Inverse scattering in elasticity—A modified gradient approach, *Wave Motion*, to appear.
15. W. H. Press, S. A. Teukolsky, W. T. Vettering, and B. P. Flannery, *Numerical Recipes in Fortran: The Art of Scientific Computing* (Cambridge Univ. Press. Cambridge, UK, 1992), 2nd ed.
16. J. H. Richmond, Scattering by a dielectric cylinder of arbitrary cross section, *IEEE Trans. Antennas Propagat.*, 334 (1965).
17. J. H. Richmond, TE wave scattering by a dielectric cylinder of arbitrary cross-section shape, *IEEE Trans. Antennas Propagat.*, 460 (1966).
18. C. H. Durney, S. C. Hill, and D. A. Chistensen, Numerical calculations of low-frequency te fields in arbitrarily shaped inhomogeneous lossy dielectric cylinders, *Radio Science* **18**, 328 (1983).
19. T. K. Sarkar, E. Arvas, and S. M. Rao, Application of the fast fourier transform and the conjugate method for efficient solution of electromagnetic scattering from both electrically large and small conducting bodies, *Electromagnetics* **5**, 99 (1985).
20. C.-T. Tsai, *Numerical Studies of Internal Field Distributions in Dielectric Bodies*, Ph.D. thesis, University of Utah, Salt Lake City, 1985.
21. P. M. van den Berg, Iterative computational techniques in scattering based upon the integrated square error criterion, *IEEE Trans. Antennas Propagat*. **AP-32** (1984).
22. P. M. van den Berg and B. J. Kooij, *Nonlinear Inversion in TE-scattering*, Technical Report, Deft University of Technology, Delft, Netherlands, 1996.
23. R. M. White, Elastic wave scattering at a cylindrical discontinuity in a solid, *J. Acoust. Soc. Am*. **30**, 771 (1958).
24. A. P. M. Zwamborn and P. M. van den Berg, A weak form of the conjugate gradient FFT method for plate problems, *IEEE Trans. Antennas Propagat*. **39**, 224 (1991).
25. A. P. M. Zwamborn and P. M. van den Berg, A weak form of the conjugate gradient FFT method for two-dimensional TE scattering problems, *IEEE Trans. Microwave Theory Tech*. **39**, 953 (1991).